Activity of metal-fluorine states upon delithiation of disordered rocksalt oxyfluorides

Indrani Roy¹, Khagesh Kumar¹, Haifeng Li¹, Neelam Sunariwal¹, Grant C.B. Alexander¹, John W. Freeland², Fanny Rodolakis², Jordi Cabana¹, *

¹ Department of Chemistry, University of Illinois Chicago, Chicago, IL, 60607, USA

² Advanced Photon Source, Argonne National Laboratory, Lemont, Illinois 60439, USA

*: corresponding author, <u>icabana@uic</u>.edu

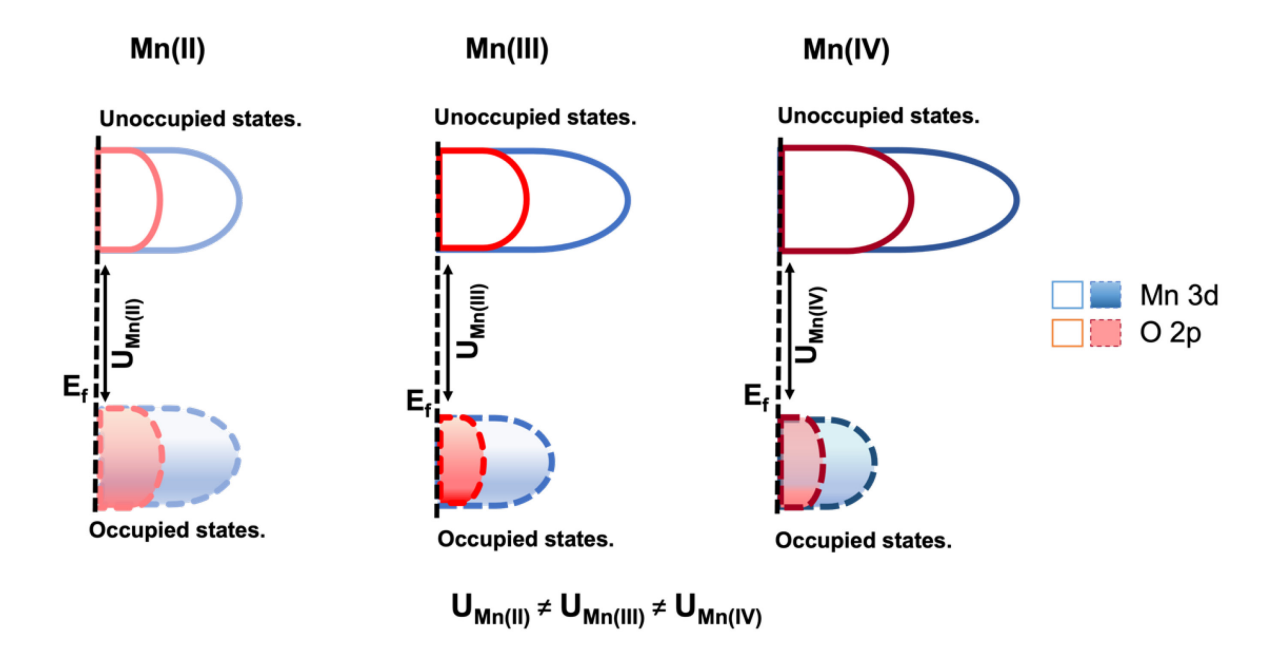
Abstract

The capacity of transition metal oxides as Li-ion battery cathodes is limited by instabilities that arise when high states of charge are achieved. Oxyfluorides with a disordered rock-salt structure have emerged as attractive alternatives, but the role of F in their electrochemical function, particularly when cationic redox produces high formal oxidation states, remains to be ascertained. Using X-ray absorption spectroscopy, we confirm the existence of Mn-F covalent interactions in Li₂MnO₂F and Li₂Mn_{2/3}Nb_{1/3}O₂F. New unoccupied states evolve from hybrid 3*d*-2*p* states of both Mn-F and Mn-O bonds when the phases are delithiated, particularly in the presence of Mn(IV). The results challenge the assumption of F as anion whose covalent states with the metal are tapped at very high potentials, providing instead a nuanced picture of redox compensation in oxyfluorides. They suggest the existence of unique knobs of design of battery cathodes by manipulating the covalent interactions between transition metals and two different anions.

Introduction:

The limitations in capacity and stability of layered oxides as cathodes for high-density Li-ion batteries motivate persistent efforts of discovery of alternative materials.¹ The discovery that Li over-stoichiometries render transition metal oxides with a disordered rock-salt structure as electroactive unlocked a vast compositional space for the potential for vertical steps in capacity and durability.² Further permutations were enabled by the substitution of O by F, a strategy with an established record in the quest for new cathode materials.³ In disordered rock-salts, this substitution is accommodated by a lower oxidation state of the metals (M) in the initial lithiated state than in the equivalent oxide, which, coupled to the Li excess, enables the reversible utilization of M(II)/M(IV) redox couples, as in Li₂Mn_{2/3}Nb_{1/3}O₂F.³ Further, the presence of F has been associated with improvements in long-term cycling stability,⁴ linked to a greater chemical,⁵ mechanical⁶ and interfacial⁷ stability of the charged (oxidized) state. However, its electronic underpinnings have not been evaluated in depth.

Cationic redox in oxides is centered on the change in electron density of M nd-O 2p hybridized states above and below the Fermi level of their band structure, which is qualitatively represented in Scheme 1. As a result, while formally described as a change in oxidation state of M, in reality, covalency dictates that the new empty states generated by oxidation always have contributions from both M and, to a greater or lesser degree, O. This fact underpins the instability of oxides when high formal oxidation states, especially Ni(IV) or Co(IV), are achieved by removal of lithium from the oxide, as it induces strong polarization of the O²- ligands, which unlocks a favorable pathway to a more reduced state through the release of heat and O2.9 More recently, redox transitions have been observed that transcend this conventional "cationic redox", whereby nonbonding O 2p states that can be tapped to induce electrochemical activity, in a process typically referred to as "lattice oxygen redox". 10 Similar changes to M nd-O 2p hybridized states have been reported for a variety of the oxyfluorides when undergoing cationic redox.^{3,11–13} In a subset of cases, lattice oxygen redox has been proposed to take place at high levels of delithiation.¹² In contrast, much less is known about the possible role of M nd-F 2p states, outside of general mentions of the existence of covalence. 14,15 Studies of Li₂MnO₂F have proposed that lattice oxygen redox is triggered before Mn environments with 3 or more F in the octahedral coordination shell can be tapped.¹¹



Scheme 1: Simplified schematics of the evolution of the projected density of the redox-active states during cationic redox in oxides. Mn is used as the example, where these states result from the overlap Mn 3d and O 2p orbitals due to covalence. The states are further split into occupied and unoccupied bands by the electron correlation, represented by the parameter U_{Mn}. This parameter will be different depending on the formal state of Mn and the specific structure of the oxide. Therefore, the scheme does not attempt to account for the magnitude of this difference for simplicity. Upon oxidation from Mn(II) to Mn(IV), the occupancy of Mn 3d-O 2p hybridized states decreases. After U is introduced, the outcome is an increase in the balance of unoccupied to occupied Mn 3d-O 2p hybridized states. No attempt was made to reflect the possible changes in relative position of the bands, as it is beyond the scope of this Scheme.

While models of the evolution of Mn-O covalence were proposed, the evolution of Mn-F bonds was not addressed.^{3,11–13} Given the high formal oxidation states reached and evidence of direct metal-fluorine bonding at high F content,¹⁶ a picture of the redox chemistry is not complete only from the evolution of metals and oxygen. The evaluation of F states is important because the stability of F⁻ anions is challenged by transition metals with a high oxidation state, especially against the late 3*d* metals common in battery cathodes.¹⁷ Indeed, in ambient conditions, MnO₂ is very stable whereas K₂MnF₆ has been used in the oxidative fluorination of graphite.¹⁸ Another open question is the balance of redox compensation between O and F states when lattice oxygen

redox is present, as has been proposed in Li₂MnO₂F and Li₂Mn_{2/3}Nb_{1/3}O₂F at high states of charge.^{3,11,12} The study of these charged oxyfluorides would create an opportunity to fundamentally understand chemical bonding between F and transition metals at high formal oxidation states, given the instability of pure fluoride counterparts, enriching our knowledge of the limits of redox chemistry in solids.^{17,19}

Here, we focus on the participation and reversibility of Mn-F states in the redox compensation of disordered oxyfluorides using Li₂MnO₂F and Li₂Mn_{2/3}Nb_{1/3}O₂F as model systems. These two compounds combine attractive cathode performance with high F contents that maximize both probability of coordination by Mn and signal quality. Since Nb has already been shown as a redox spectator,³ we follow the evolution of Mn, O and F using X-ray absorption spectroscopy (XAS). While the results with Mn and O were in agreement with the literature,^{3,12} we also show that F not only engages in Mn 3*d*-F 2*p* covalent bonding but that such covalency evolves with the formal oxidation state of Mn from the early stages of delithiation. This study enriches evaluations in the literature of these same compounds by uncovering the active role of Mn 3*d*-F 2*p* hybridization in the operation of these attractive oxyfluorides. Since F actively contributes to the electrochemical performance of these novel cathode materials, there are implications for stability, particularly given the possibility of unusual Mn(IV)-F interactions, that should be evaluated in future work.

Experimental Section:

Synthesis

Li₂MnO₂F and Li₂Mn_{2/3}Nb_{1/3}O₂F were synthesized by high-energy ball milling following the procedure reported by Lun et. al.¹³ and Lee et. al.,²⁰ respectively. Li₂O (Alfa Aesar, ACS, 99% min), MnO (Sigma-Aldrich, 99.99%), Mn₂O₃ (Alfa Aesar, 99%), Nb₂O₅ (Sigma-Aldrich, 99.99%) and LiF (Alfa Aesar, 99.99%) were used as precursors. The precursors were mixed in stochiometric proportions with a Retsch PM 200 planetary ball mill at a rate of 300 rpm for 2 h, in argon-filled stainless-steel ball-mill jars. The grinding media were five 10 mm (diameter) stainless balls and ten 5 mm (diameter) balls. The total amount of precursors was 1 g. To induce the desired reaction, the mixed precursors were subsequently ball-milled at 500 rpm, with all other parameters

staying the same. The duration of the treatment was 40 h and 50 h for Li_2MnO_2F and $Li_2Mn_{2/3}Nb_{1/3}O_2F$, respectively.

Electrochemistry

Powder electrodes were prepared by ball-milling the active material with conductive carbon (Super C65 from Imerys, typical Fe content of 2 ppm) for 3 h at 300 rpm. The ratios of active material to carbon were 85:15 and 70:30 for Li₂MnO₂F and Li₂Mn_{2/3}Nb_{1/3}O₂F, respectively. We refrained from preparing composite electrode to reduce the interference from F species present in fluorinated binders during spectroscopic analysis.

All the cells were fabricated in an argon-filled glove box (< 0.1 ppm of both H₂O and O₂). The cell was composed of the positive electrode and a high-purity lithium foil (Alfa Aesar) as the counter/pseudo-reference electrode, separated by a Whatman GF/D borosilicate glass fiber membrane, impregnated with 1 M LiPF₆ dissolved in a mixture of ethylene carbonate (EC)/ethyl methyl carbonate (EMC) (3:7, wt%/wt%). The galvanostatic charge–discharge cycling was performed at room temperature using a BT-Lab tester (Bio-Logic) with a current rate of C/20 (indicating 1 mol Li per formula unit is extracted in 20 hours) at different cutoff voltages. All potentials quoted in this paper were referenced to Li⁺/Li⁰ unless otherwise mentioned. Upon arriving at the state of interest, the cell was immediately stopped and disassembled in the argon-filled glovebox to avoid self-discharging under open-circuit state. Then, the cycled powders were harvested, followed by drying under vacuum in the glovebox antechamber for 30 minutes. Dried electrodes were stored in the argon-filled glovebox for ex situ characterization.

Characterization

Ex situ diffraction: Laboratory powder X-ray diffraction (pXRD) profiles were collected by scanning from 10° to 90° , 2θ , using a step size of 0.019° , at a rate of $2.6x10-5^{\circ}$ /min 2θ , in a custom air-free sample holder, in a Bruker D8 Advance diffractometer operating at 40 kV and 40 mA with Cu K α radiation ($\lambda = 1.5418 \text{ Å}$).

X-ray absorption spectroscopy: O K-edge, F K-edge, and Mn $L_{2,3}$ -edge X-ray absorption spectroscopy (XAS) data was collected *ex situ* at beamline 29-ID-D of the Advance Photon Source (APS) at Argonne National Laboratory. Samples of interest were attached to a copper sample holder using conductive carbon tape in an argon-filled glovebox and then transferred into an X-

ray absorption antechamber through an argon environment to minimize the potential exposure to air. Data were measured under total fluorescence yield (TFY) mode using a silicon drift diode detector (Vortex). Data was obtained at a spectral resolution of ~ 0.1 eV, with a 1 s dwelling time. During the measurement, three scans were performed at each absorption edge, and scans were then averaged to maximize the signal-to-noise ratio.

During the measurement, the XAS spectra were recorded over a wide energy range to cover energies well below and above sample absorptions. Normalization was conducted by dividing each curve by the dataset mean value.

Results and Discussion:

The two compounds were synthesized by ball-milling and crystallized in a disordered oxyfluoride structure (Figure S1). The XRD results were found to be consistent with the literature^{3,12} confirms that all the synthesized materials form a disordered rock-salt structure. Both materials were cycled in Li metal half-cells (Figure S2), with responses similar to the literature.^{3,12} The redox mechanism of the materials was investigated using X-ray absorption spectroscopy (XAS) at the Mn L-edge, O and F K-edge. Unless otherwise indicated, spectra correspond to total fluorescence yield (TFY) detection, probing into sufficient depth (~100 nm) to represent the bulk of the compounds.

We start our analysis with the evolution of Mn and O. Figure 1(a,b) shows the Mn L_{2,3}-edge XAS of Li₂MnO₂F and Li₂Mn_{2/3}Nb_{1/3}O₂F at various charge and discharge stages, compared to reference compounds with known Mn redox state. Li₂MnO₂F has Mn L_{2,3} features consistent with Mn(III) (Figure 1a), particularly a center of gravity around 643eV, whereas the dominance of a narrow feature at 642 eV is an indication of Mn(II) in Li₂Mn_{2/3}Nb_{1/3}O₂F (Figure 1b). Charging of both electrodes induced a gradual shift of the Mn L_{2,3}-edge towards higher energy, with dominant features at 645 eV and an L₂-edge centered at 655 eV, indicating the formation of Mn(IV) (Figures 1a,b). Oxidation of Mn appeared to be arrested for Li₂MnO₂F at 4.6 V, consistent with the fact that Mn(IV) cannot be further oxidized at these potentials.²¹ Full oxidation to Mn(IV) required Li₂Mn_{2/3}Nb_{1/3}O₂F charging above 4.8 V. The persistence of high intensity around 642 eV in the

most charged states of both Li₂MnO₂F and Li₂Mn_{2/3}Nb_{1/3}O₂F suggests the possibility of Mn(II) being present. In the case of Li₂Mn_{2/3}Nb_{1/3}O₂F, it could signal an incomplete oxidation of all Mn. This explanation is less parsimonious for Li₂MnO₂F, since it starts as Mn(III). It is possible that there are competing processes during charging that produce Mn(II) locally or that such Mn(II) signals are due to an impurity that could not be detected in the pristine state by XRD and/or XAS due to low crystallinity and the dominance of Mn(III) signals, respectively. The origin of these inefficiencies should be explored in future work. Sharpe et al. proposed that Mn cannot be fully oxidized before lattice oxygen redox is triggered.¹¹ Supplementary Mn K-edge XAS measurements of both compounds confirmed the trends of redox revealed by the Mn L_{2,3}-edge (Figure S3). In general, all trends followed closely with the observations in the literature^{13,20,22}.

O K-edge XAS probes dipole-allowed transitions from core O 1s to empty O 2p states. The spectra (Figures 1(c,d)) are divided into pre-edge and edge regions, below and above 535 eV, respectively. The pre-edge (<535 eV) represents the unoccupied states resulting from O 2p orbitals hybridized with Mn 3d orbitals, and the broad band above 535 eV corresponds to a collection of excitations from O 1s to orbital to empty states of O 2p orbitals mixed with the TM 4s and 4p orbitals, and ultimately, the continuum. The clearest changes were seen at the pre-edge. The existence of multiple spectral features below 535 eV in pristine Li₂MnO₂F (Figure 1c) reflects a low degeneracy of O 2p-Mn 3d states, consistent with Mn(III) in local environments with coordination number 6, but distorted by the Jahn-Teller effect.²³ In turn, the redshift of the preedge and its simpler line shape after oxidation to 4.6 V is consistent with formation of an octahedral (Mn(IV)-O₆) arrangement, where the two main components are commonly assigned to unoccupied t_{2g} and e_g states.²⁴ This change of the pre-edge is a signature of the participation of O in the new covalent states generated to compensate the charging of the oxyfluoride cathode, as depicted in Scheme 1. Little change was observed on further oxidation at 4.8 V, except for a subtle increase in relative intensity at 531.5 eV associated to lattice oxygen redox by House et al., ¹² thus explaining the lack of change at the Mn $L_{2,3}$ -edge.

Comparison of the pre-edge signals of Li₂Mn_{2/3}Nb_{1/3}O₂F (Figure 1d) with MnO and Nb₂O₅ in the literature²⁵, indicated hybridization between O 2*p* states and both Mn 3*d* and Nb 4*d*. A preference for bonds between O²⁻ and Nb(V) would be predicted based on trends derived by Fuertes based on Pauling's second rule,²⁶ whereby cations and anions in a mixed anion compound

tend to associate according to the size of their charge. The pre-edge peak at 532.5 eV did not undergo significant changes in any of the electrodes, consistent with an assignment to Nb(V)-O states, which are redox spectators. Rather, there was a progressive increase in intensity in a shoulder at 530 eV, all the way to 4.8 V, as expected for the oxidation to Mn(IV), and reminiscent of the changes at similar states in Li₂MnO₂F. These observations also agree well with previous reports.^{3,12,13}

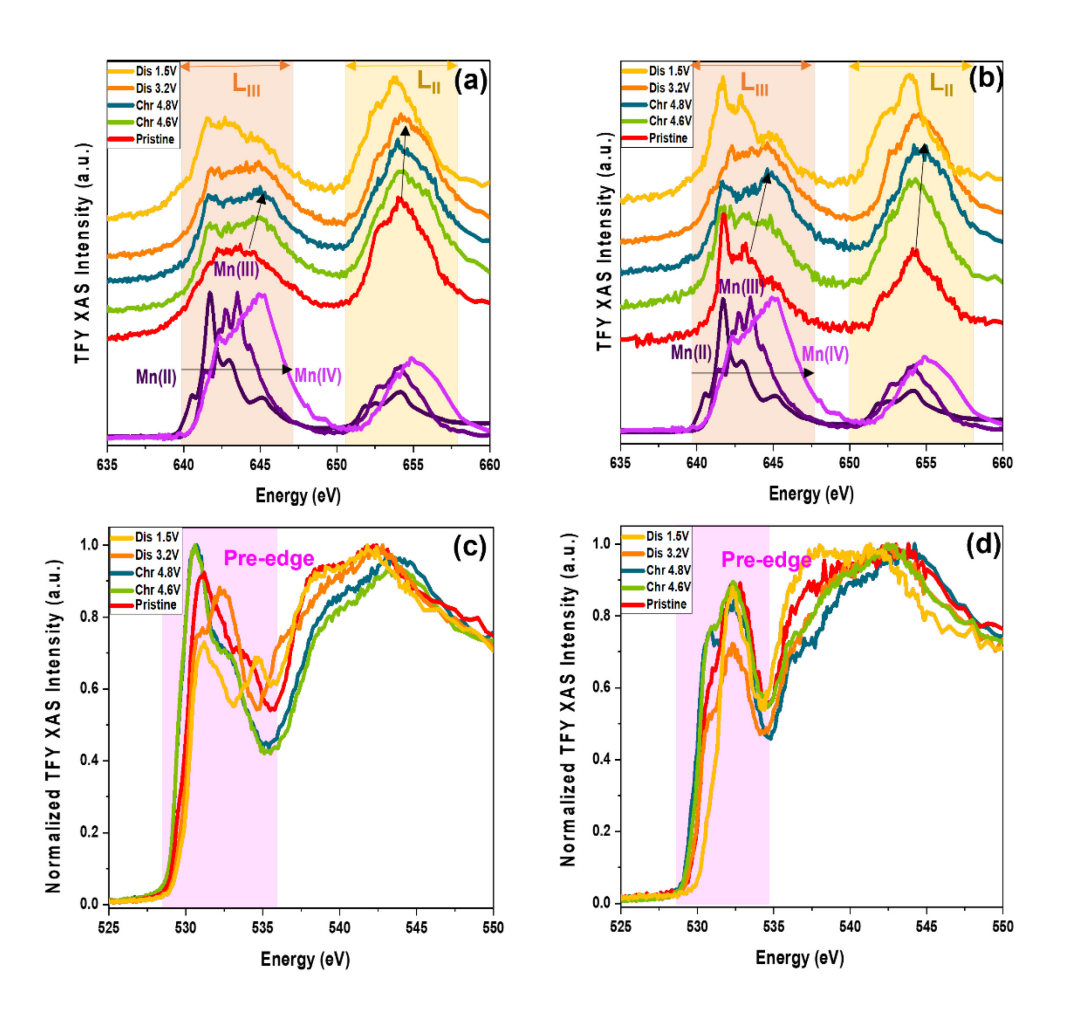


Figure 1: Ex situ (a-b) Mn $L_{2,3}$ -edge and (c-d) O K-edge XAS of (a, c) Li_2MnO_2F and (b, d) $Li_2Mn_{2/3}Nb_{1/3}O_2F$ at different states, measured in total fluorescence yield (TFY) mode. Labels: chr=charge, dis=discharge.

Like O, the F K-edge XAS of Li₂MnO₂F (Figure 2(a)) also presented a clear pre-edge feature (<690 eV), followed by the absorption edge, a broad band above 690 eV. No intensity was observed below 690 eV in the spectrum of LiF²⁷ (Figure 2(a)), but it was above the background for MnF₂ and, especially, MnF₃ reference compounds (Figure S4). Therefore, it is safe to conclude that the pre-edge in these oxyfluorides arises from unoccupied states involving hybridization of F 2p and Mn 3d states, also in agreement with previous general observations of transition metal fluorides.^{28,29} The results confirm the existence of covalent bonds between Mn(III) and F in this compound.¹¹ The pre-edge intensity was much lower in Li₂Mn_{2/3}Nb_{1/3}O₂F, but persistent when compared with LiF²⁷ (Figure 2(b)). The much lower intensity at this energy in Li₂Mn_{2/3}Nb_{1/3}O₂F than Li₂MnO₂F is expected from interactions between Mn(II) and F that are less covalent than with Mn(III), based on basic arguments of polarizing power of the cation. Li₂Mn_{2/3}Nb_{1/3}O₂F displays cation and anion disorder, but the trends established by Fuertes²⁶ predict that the cation with higher charge will have greater tendency to locally cluster with anions of higher charge. Thus, the probability of Nb(V)-F bonds would be lower than Nb(V)-O bonds, in line with predictions for related disordered rocksalts.¹⁶

When Li₂MnO₂F was oxidized to 4.6 V, new signals emerged at ~686 eV, leading to an increased pre-edge intensity overall. The edge, above 690 eV, notably broadened. Further oxidation of Li₂MnO₂F to 4.8V further broadening of the signals riding on the absorption edge, with an increased intensity at 689 eV. In turn, by removing ~0.7 mol of Li⁺ per formula unit from Li₂Mn_{2/3}Nb_{1/3}O₂F to 4.6V (Figure S2), a slight gain in intensity was observed below 690 eV, alongside a broadening of the edge. A pre-edge peak at ~687 eV became prominent with further charging to 4.8 V.

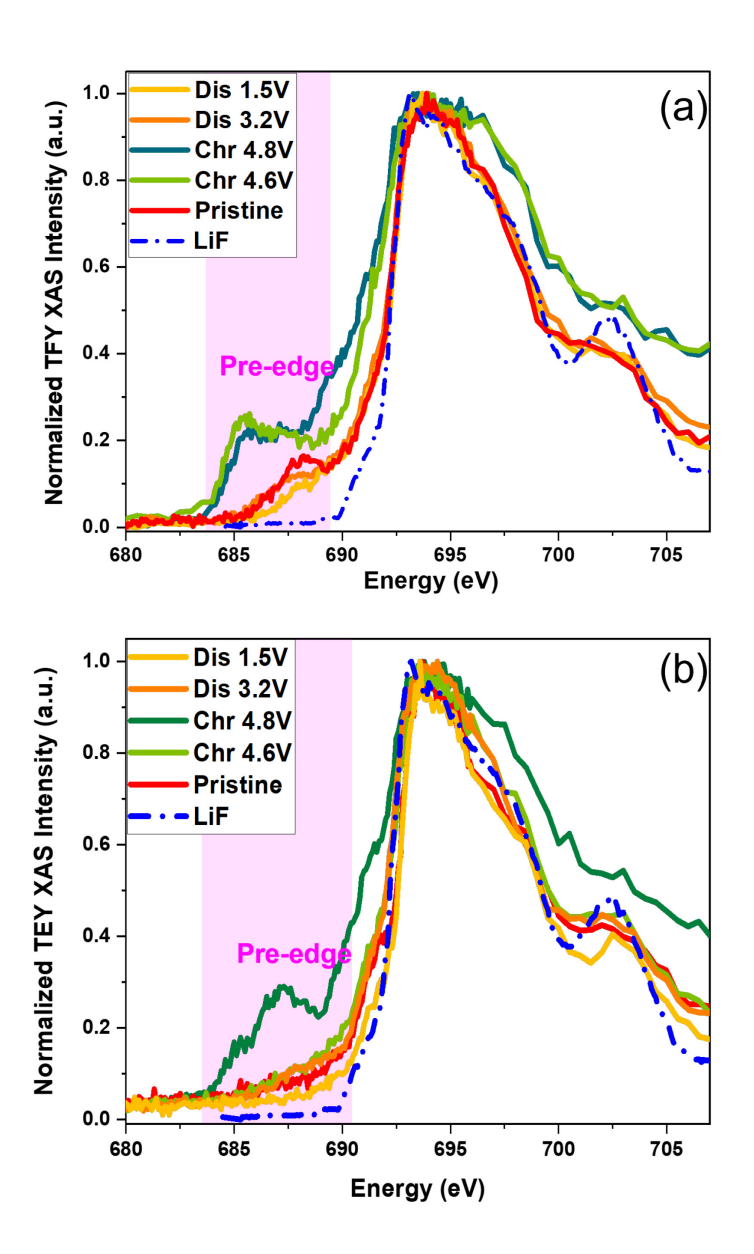


Figure 2: *Ex situ* F K-edge XAS of (a) Li₂MnO₂F and (b) Li₂Mn_{2/3}Nb_{1/3}O₂F at different states, measured in total fluorescence yield (TFY) mode. The spectra are compared to LiF²⁷ to provide a clear contrast of the pre-edge signals below 690 eV. Representative electrochemical profiles are found in Figure S2. Labels: chr=charge, dis=discharge.

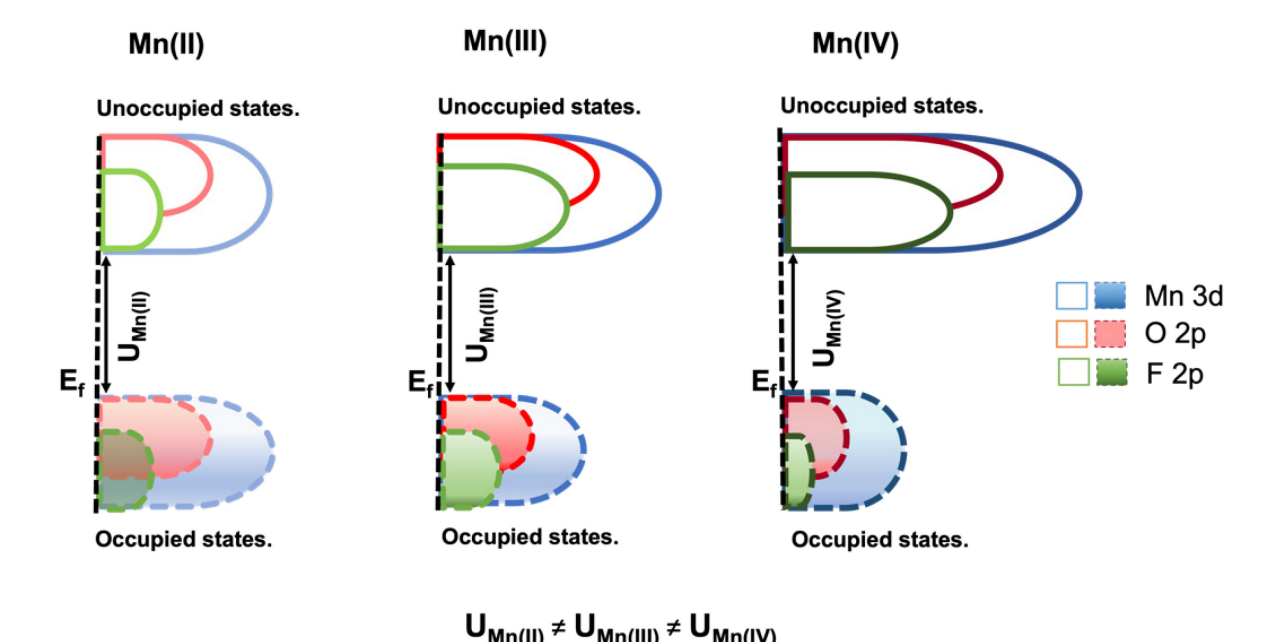
These electrodes did not contain fluorinated binders, but since they were exposed to the electrochemical cell environment, consideration was given to the hypothesis that fluorinated species from the electrolyte could contribute, especially upon decomposition at high potential.

Several analyses exist in the literature of the F K-edge signatures of LiPF₆ in the electrolyte and the products of its decomposition on cathodes operating at high potential. ^{30–34}Like LiF²⁷, none of the species in the literature had signals below 690 eV, and, therefore, no measurable pre-edge. We also measured F K-edge XAS of all harvested electrodes in total electron yield (TEY, Figure S5), which only probes ~10nm into the surface and, thus, has much more significant contributions the products of deleterious interfacial reactions upon cycling than TFY XAS. ^{14,15} In all cases, the pre-edge signals below 690 eV were much weaker in TEY than TFY measurements. This observation confirms that species arising from electrolyte decomposition on the electrode surface, which are dominant in the TEY spectra of the cycled cathodes, do not have prominent pre-edge signals, consistent with the literature^{30–34}.

Therefore, the increase in F pre-edge signals upon charging Li₂MnO₂F and Li₂Mn_{2/3}Nb_{1/3}O₂F undeniably shows that new unoccupied Mn-F states result from oxidation of the compound, thus indicating that they are involved in charge compensation. Species arising from electrolyte processes do not have as elevated intensity at the onset of the edge, around 690 eV (see TEY in Figure S5)^{30–34}, as we found at the highest states of charge in TFY XAS (Figure 2), suggesting the edge broadening also arises from the oxidation of the bulk oxyfluoride. But this assignment is less certain than in the case of the pre-edge and merits further investigation.

The F, O and Mn changes produced after charge were progressively undone upon discharge to 1.5 V. However, some evidence of irreversibility was found when comparing pristine and fully discharged states. In the F K-edge XAS (Figure 2), the intensity at the pre-edge was lower in the discharged than the pristine state of both Li₂MnO₂F and Li₂Mn_{2/3}Nb_{1/3}O₂F. In the case of Li₂MnO₂F, this change was coupled with a high intensity at 642 eV (Mn L₃-edge, Figure 1a) and a new peak at 535 eV (O K-edge, Figure 1c). These three changes were ascribed to an over-reduction of the oxyfluoride, producing signals from both Mn(III)-O/F and Mn(II)-O/F states. In turn, the other most obvious difference in Li₂Mn_{2/3}Nb_{1/3}O₂F was the lower relative intensity at 530 eV in the O K-edge of the discharged versus pristine states (Figure 1d), an irreversibility of unclear origin, considering that the Mn L_{2,3}-edge did not reveal reduction below Mn(II). Lee *et al.*³ posited the existence of changes of local coordination of Mn and Nb upon cycling based on K-edge data, which would affect the hybridization with O and F and, thus, the relative distribution of pre-edge signals in the corresponding spectra.

Scheme 2 presents a qualitative picture of bonding that emerges from our results, expanding the established understanding of cationic redox in pure oxides. For simplicity, only the frontier O/F 2p-Mn 3d orbitals are represented, since they are the primary compensation centers. For instance, the diagram does not depict the predicted formation of states close to the Fermi level that arise from O-O dimerization in this compound, as described by Sharpe et al.¹¹ According to XAS, conventional oxidation of Mn operates until Mn(IV) is reached. Pre-edge signals at the F K-edge were apparent in the presence of Mn(III). In consequence, the Scheme 2 reflects the depopulation of O and F 2p- Mn 3d states from early stages of reaction, rather than F only being, at most, accessible upon extreme values of delithiation.¹¹ In Li₂MnO₂F, charging beyond 4.6 V triggers lattice oxygen redox, 12 yet the F K-edge XAS continues to evolve, suggesting that such unconventional redox affects F as well. In fact, the changes from 4.6 V to 4.8 V, where an equivalent 1.25 mol Li have been deintercalated per mol Li₂MnO₂F, appear even more pronounced at the F K- than both Mn L_{2,3}- and O K-edges. The growth of F K-edge signals close to the absorption edge (at ~690 eV) during this process, rather than the pre-edge (<690 eV), indicates a non-trivial process may be occurring for the halide. Given this fact, and to avoid excessive speculation, the band structure at this charged state is not depicted in Scheme 1. The notable evolution of F K-edge is not observed at the surface (TEY spectra in Figure S5), again indicating a process in the bulk of the oxyfluoride.



Scheme 2: Simplified schematics of the proposed evolution of the projected density of the unoccupied Mn 3*d*-O/F 2*p* states in Li_{2-x}MnO₂F and Li_{2-x}Mn_{2/3}Nb_{1/3}O₂F with *x*. They qualitatively reflect the participation of Mn, O and F in the redox transitions, consistent with the XAS data in Figures 1 and 2. The F bands are depicted at lower energy based on computational predictions of redox potentials. The Mn 3*d*-O/F 2*p* states are split into occupied and unoccupied bands by the electron correlation, represented by the parameter U_{Mn}. This parameter will be different depending on the formal state of Mn, which was not directly measured in our work. Thus, the scheme does not account for its change with oxidation state for simplicity. Upon oxidation from Mn(II) to Mn(IV), the occupancy of redox-active states decreases. After U is introduced, the outcome is an increase in the balance of unoccupied to occupied states. According to the results presented here, all three unoccupied bands increase in density, which raises the intensity of the pre-edge in O and F K-edge XAS. The diagrams also show a hypothetical change in the corresponding occupied bands (dashed line), simply to mimic Scheme 1 and reflect an expected decrease in density for the three elements as they are depopulated. No attempt was made to reflect the possible changes in relative position of the bands, as it is beyond the scope of this Scheme.

Conclusion:

This study shows that F states actively participate upon cationic redox in oxyfluoride cathodes with a disordered structure, even at relatively low states of charge. Specifically, delithiation of Li₂MnO₂F and Li₂Mn_{2/3}Nb_{1/3}O₂F affects the covalent bond between Mn 3*d* states and both O and F 2*p* states. The existence of charge compensation at F has implications for the stability of the compounds in their oxidized state which should be evaluated in view of their application as cathodes. Further insight into the exact states that lead to this behavior will require sophisticated computations of the electronic structure and, ideally, modeling of the XAS, especially to probe the observations during lattice oxygen redox. This work opens fresh lines of inquiry and degrees of freedom in the redox behavior of mixed anion compounds. Broadening the design rules to consider the participation of F could be leveraged to design new cathode materials for high-energy Li-ion batteries displaying metrics that transcend current candidates.

Supporting Information:

The supporting information includes XRD of Li₂MnO₂F and Li₂Mn_{2/3}Nb_{1/3}O₂F, Electrochemical profile of the first cycle of Li₂MnO₂F and Li₂Mn_{2/3}Nb_{1/3}O₂F, Mn K-edge XAS of the various

charge and discharged states of Li₂MnO₂F and Li₂Mn_{2/3}Nb_{1/3}O₂F, comparison of the F K-edge XAS of LiF, MnF₂ and MnF₃ with pristine Li₂MnO₂F and Li₂Mn_{2/3}Nb_{1/3}O₂F.

Acknowledgements:

This material is based upon work supported by the National Science Foundation under Grant No. DMR- 2118020. This research used resources of the Advanced Photon Source; a U.S. Department of Energy (DOE) Office of Science User Facility operated for the DOE Office of Science by Argonne National Laboratory under Contract No. DE-AC02-06CH11357.

Bibliography:

- (1) Myung, S. T.; Maglia, F.; Park, K. J.; Yoon, C. S.; Lamp, P.; Kim, S. J.; Sun, Y. K. Nickel-Rich Layered Cathode Materials for Automotive Lithium-Ion Batteries: Achievements and Perspectives. ACS Energy Lett. 2017, 2 (1), 196–223.
- (2) Clément, R. J.; Lun, Z.; Ceder, G. Cation-Disordered Rocksalt Transition Metal Oxides and Oxyfluorides for High Energy Lithium-Ion Cathodes. *Energy Environ. Sci.* **2020**, *13* (2), 345–373.
- (3) Lee, J.; Kitchaev, D. A.; Kwon, D. H.; Lee, C. W.; Papp, J. K.; Liu, Y. S.; Lun, Z.; Clément, R. J.; Shi, T.; McCloskey, B. D.; Guo, J.; Balasubramanian, M.; Ceder, G. Reversible Mn²⁺/Mn⁴⁺ Double Redox in Lithium-Excess Cathode Materials. *Nature.* 2018 5567700 2018, 556 (7700), 185–190.
- (4) Lee, J.; Papp, J. K.; Clément, R. J.; Sallis, S.; Kwon, D. H.; Shi, T.; Yang, W.; McCloskey, B. D.; Ceder, G. Mitigating Oxygen Loss to Improve the Cycling Performance of High Capacity Cation-Disordered Cathode Materials. *Nat. Commun.* 2017 81 2017, 8 (1), 1–10.
- (5) Lun, Z.; Ouyang, B.; Kitchaev, D. A.; Clément, R. J.; Papp, J. K.; Balasubramanian, M.; Tian, Y.; Lei, T.; Shi, T.; McCloskey, B. D.; Lee, J.; Ceder, G. Improved Cycling Performance of Li-Excess Cation-Disordered Cathode Materials upon Fluorine

- Substitution. Adv. Energy Mater. 2019, 9 (2), 1802959.
- (6) Chen, D.; Zhang, J.; Jiang, Z.; Wei, C.; Burns, J.; Li, L.; Wang, C.; Persson, K.; Liu, Y.; Chen, G. Role of Fluorine in Chemomechanics of Cation-Disordered Rocksalt Cathodes. *Chem. Mater.* **2021**, *33* (17), 7028–7038.
- (7) Li, L.; Lun, Z.; Chen, D.; Yue, Y.; Tong, W.; Chen, G.; Ceder, G.; Wang, C. Fluorination-Enhanced Surface Stability of Cation-Disordered Rocksalt Cathodes for Li-ion Batteries. *Adv. Funct. Mater.* **2021**, *31* (25), 2101888.
- (8) Yoon, W. S.; Balasubramanian, M.; Chung, K. Y.; Yang, X. Q.; McBreen, J.; Grey, C. P.; Fischer, D. A. Investigation of the Charge Compensation Mechanism on the Electrochemically Li-ion Deintercalated Li_{1-X}Co_{1/3}Ni_{1/3}Mn_{1/3}O₂ Electrode System by Combination of Soft and Hard X-Ray Absorption Spectroscopy. *J. Am. Chem. Soc.* **2005**, *127* (49), 17479–17487.
- (9) Liu, X.; Ren, D.; Hsu, H.; Feng, X.; Xu, G. L.; Zhuang, M.; Gao, H.; Lu, L.; Han, X.; Chu, Z.; Li, J.; He, X.; Amine, K.; Ouyang, M. Thermal Runaway of Lithium-Ion Batteries without Internal Short Circuit. *Joule* **2018**, *2* (10), 2047–2064.
- (10) Gent, W. E.; Abate, I. I.; Yang, W.; Nazar, L. F.; Chueh, W. C. Design Rules for High-Valent Redox in Intercalation Electrodes. *Joule* **2020**, *4* (7), 1369–1397.
- (11) Sharpe, R.; House, R. A.; Clarke, M. J.; Förstermann, D.; Marie, J. J.; Cibin, G.; Zhou, K. J.; Playford, H. Y.; Bruce, P. G.; Islam, M. S. Redox Chemistry and the Role of Trapped Molecular O₂ in Li-Rich Disordered Rocksalt Oxyfluoride Cathodes. *J. Am. Chem. Soc.* 2020, 142 (52), 21799–21809.
- (12) House, R. A.; Jin, L.; Maitra, U.; Tsuruta, K.; Somerville, J. W.; Fö Rstermann, D. P.; Massel, F.; Duda, L.; Roberts, M. R.; Bruce, P. G. Lithium Manganese Oxyfluoride as a New Cathode Material Exhibiting Oxygen Redox. *Energy Environ. Sci* **2018**, *11*, 926.
- (13) Lun, Z.; Ouyang, B.; Cai, Z.; Clément, R. J.; Kwon, D. H.; Huang, J.; Papp, J. K.; Balasubramanian, M.; Tian, Y.; McCloskey, B. D.; Ji, H.; Kim, H.; Kitchaev, D. A.; Ceder, G. Design Principles for High-Capacity Mn-Based Cation-Disordered Rocksalt Cathodes. *Chem* 2020, 6 (1), 153–168.

- (14) Ahn, J.; Chen, D.; Chen, G. A Fluorination Method for Improving Cation-Disordered Rocksalt Cathode Performance. *Adv. Energy Mater.* **2020**, *10* (35), 2001671.
- (15) Yue, Y.; Ha, Y.; Giovine, R.; Clément, R.; Yang, W.; Tong, W. High-Voltage Reactivity and Long-Term Stability of Cation-Disordered Rocksalt Cathodes. *Chem. Mater.* **2022**, *34* (4), 1524–1532.
- (16) Ji, H.; Kitchaev, D. A.; Lun, Z.; Kim, H.; Foley, E.; Kwon, D. H.; Tian, Y.; Balasubramanian, M.; Bianchini, M.; Cai, Z.; Clément, R. J.; Kim, J. C.; Ceder, G. Computational Investigation and Experimental Realization of Disordered High-Capacity Li-Ion Cathodes Based on Ni Redox. *Chem. Mater.* 2019, 31 (7), 2431–2442.
- (17) Riedel, S.; Kaupp, M. The Highest Oxidation States of the Transition Metal Elements. *Coord. Chem. Rev.* **2009**, *253* (5–6), 606–624.
- (18) Lemmon, J. P.; Lerner, M. M. Synthesis of Planar-Sheet Graphite Fluorides Using Fluorometallate Salts of Transition Metals in Anhydrous Hydrogen Fluoride. *Carbon* **1993**, *31* (3), 437–443.
- (19) Dimov, N.; Nishimura, A.; Chihara, K.; Kitajou, A.; Gocheva, I. D.; Okada, S. Transition Metal NaMF₃ Compounds as Model Systems for Studying the Feasibility of Ternary Li-M-F and Na-M-F Single Phases as Cathodes for Lithium–Ion and Sodium–Ion Batteries. Electrochim. Acta 2013, 110, 214–220.
- (20) Lee, J.; Kitchaev, D. A.; Kwon, D.; Lee, C.; Papp, J. K.; Liu, Y.; Lun, Z. Lithium-Excess Cathode Materials. *Nature* **2018**, *556*, 185–190.
- (21) Rana, J.; Papp, J. K.; Lebens-Higgins, Z.; Zuba, M.; Kaufman, L. A.; Goel, A.; Schmuch, R.; Winter, M.; Whittingham, M. S.; Yang, W.; McCloskey, B. D.; Piper, L. F. J. Quantifying the Capacity Contributions during Activation of Li₂MnO₃. *ACS Energy Lett.* **2020**, *5* (2), 634–641.
- (22) Clément, R. J.; Lun, Z.; Ceder, G. Cation-Disordered Rocksalt Transition Metal Oxides and Oxyfluorides for High Energy Lithium-Ion Cathodes. *Energy Environ. Sci*, 2020, 345–373.
- (23) Noh, H. J.; Yeo, S.; Kang, J. S.; Zhang, C. L.; Cheong, S. W.; Oh, S. J.; Johnson, P. D.

- Jahn-Teller Effect in Spinel Manganites Probed by Soft X-Ray Absorption Spectroscopy. *Appl. Phys. Lett.* **2006**, *88* (8), 081911.
- (24) Abbate, M.; De Groot, F. M. F.; Fuggle, J. C.; Fujimori, A.; Strebel, O.; Lopez, M. F.; Domke, M.; Kaindl, G.; Sawatzky, G. A.; Takano, M.; Takeda, Y.; Eisaki, H.; Uchida, S. Controlled-Valence Properties of La_{1-X}Sr_xFeO₃ and La_{1-X}Sr_xMnO₃ Studied by Soft X-Ray Absorption Spectroscopy. *Phys. Rev. B* **1992**, *46* (8), 4511–4519.
- (25) Frati, F.; Hunault, M. O. J. Y.; De Groot, F. M. F. Oxygen K-Edge X-Ray Absorption Spectra. *Chem. Rev.* **2020**, *120* (9), 4056–4110.
- (26) Fuertes, A. Prediction of Anion Distributions Using Pauling's Second Rule. *Inorg. Chem.* **2006**, *45* (24), 9640–9642.
- (27) Kuhn, A.; Plews, M. R.; Pérez-Flores, J. C.; Fauth, F.; Hoelzel, M.; Cabana, J.; García-Alvarado, F. Redox Chemistry and Reversible Structural Changes in Rhombohedral VO₂F Cathode during Li Intercalation. *Inorg. Chem.* **2020**, *59* (14), 10048–10058.
- (28) Bondino, F.; Malvestuto, M.; Magnano, E.; Zangrando, M.; Zacchigna, M.; Ghigna, P.; Parmigiani, F. Overlap of Cu 3d and F 2p Orbitals and Low-Energy Excitations in KCuF₃ Studied by Polarization-Dependent x-Ray Absorption and Emission Spectroscopy. *Phys. Rev. B Condens. Matter Mater. Phys.* **2009**, *79* (11), 115120.
- (29) Olalde-Velasco, P.; Jiménez-Mier, J.; Denlinger, J. D.; Hussain, Z.; Yang, W. L. Direct Probe of Mott-Hubbard to Charge-Transfer Insulator Transition and Electronic Structure Evolution in Transition-Metal Systems. *Phys. Rev. B - Condens. Matter Mater. Phys.* 2011, 83 (24), 241102.
- (30) Schellenberger, M.; Golnak, R.; Quevedo Garzon, W. G.; Risse, S.; Seidel, R. Accessing the Solid Electrolyte Interphase on Silicon Anodes for Lithium-Ion Batteries in-Situ through Transmission Soft X-Ray Absorption Spectroscopy. *Mater. Today Adv.* **2022**, *14*, 100215.
- (31) Hasa, I.; Haregewoin, A. M.; Zhang, L.; Tsai, W. Y.; Guo, J.; Veith, G. M.; Ross, P. N.; Kostecki, R. Electrochemical Reactivity and Passivation of Silicon Thin-Film Electrodes in Organic Carbonate Electrolytes. *ACS Appl. Mater. Interfaces* **2020**, *12* (36), 40879–

40890.

- (32) Balasubramanian, M.; Lee, H. S.; Sun, X.; Yang, X. Q.; Moodenbaugh, A. R.; McBreen, J.; Fischer, D. A.; Fu, Z. Formation of SEI on Cycled Lithium-Ion Battery Cathodes Soft X-Ray Absorption Study. *Electrochem. Solid-State Lett.* 2002, 5 (1), A22.
- (33) Hestenes, J. C.; May, R.; Sadowski, J. T.; Munich, N.; Marbella, L. E. Resolving Chemical and Spatial Heterogeneities at Complex Electrochemical Interfaces in Li-Ion Batteries. *Chem. Mater.* **2022**, *34* (1), 232–243.
- (34) Chung, K. Y.; Yoon, W. S.; Kim, K. B.; Cho, B. W.; Yang, X. Q. Formation of an SEI on a LiMn₂O₄ Cathode during Room Temperature Charge-Discharge Cycling Studied by Soft X-Ray Absorption Spectroscopy at the Fluorine K-Edge. *J. Appl. Electrochem.* **2011**, *41* (11), 1295–1299.

TOC figure:

